





Correlation of spin-orbit potential and effective mass

N. N. Arsenyev ¹, A. P. Severyukhin ^{1,2}, G. G. Adamian ¹ and N. V. Antonenko ¹

¹*Joint Institute for Nuclear Research, 141980 Dubna, Moscow region, Russia*

²*Dubna State University, 141982 Dubna, Moscow region, Russia*



(Received 1 March 2024; revised 17 July 2024; accepted 14 August 2024; published 11 September 2024)

The correlation between the spin-orbit strength and effective mass at saturation density is demonstrated for various Skyrme energy-density functionals without tensor force. This correlation can be used to reduce the number of parameters in these functionals. The role of the spin-orbit interaction is considered together with the tensor force, which has a similar effect on the observable nuclear characteristics. The use of the relation obtained between the spin-orbit strength and the effective mass in the calculations of binding energies, spin-orbit splitting, and charge radii does not spoil the description of experimental data.

DOI: [10.1103/PhysRevC.110.034312](https://doi.org/10.1103/PhysRevC.110.034312)

I. INTRODUCTION

The spin-orbit interaction strongly affects the nuclear structure [1–3]: shell closures appear at certain magic neutron N and proton Z numbers. A change in the strength of the spin-orbit interaction by about 20% results in a different shell closure (at $Z = 114$ or 120) in superheavy nuclei [4]. The shell evolution in the isotopic chain also crucially depends on the spin-orbit interaction [5]. The reduction of spin-orbit coupling in neutron-rich nuclei and a quenching of shell effects due to the interaction with continuum were extensively discussed in Refs. [6,7].

In addition to the spin-orbit interaction, the tensor force influences the splitting of single-particle levels [8]. As shown in Refs. [9,10], in the approach using bare nucleon-nucleon interaction, nuclei are unbound without taking into account two-body correlations through the tensor force. The tensor terms of the energy density functional (EDF) can contribute as much to the spin-orbit splitting as to the spin-orbit force. The spin-orbit splitting in the single-particle spectra should be discussed along with the tensor force. Although many effective Skyrme EDFs omit the tensor force, its effect is hidden in the parameters of the spin-orbit interaction or in the finite-range effect. As a result, there is a correlation between the constant W_0 of the spin-orbit force and the strength of the tensor force. The tensor force has the tendency to reduce the spin-orbit splittings in spin-unsaturated nuclei. To keep the spin-orbit splitting, the value of W_0 has to be increased. The value of W_0 correlates with the isoscalar tensor coupling C_0^J [8] so that the single-particle spectra obtained with T24 and T42 EDFs are similar to those for T26, T44, and T62 EDFs in which the W_0 values are about 12% larger and the C_0^J values are twice as large. So the change of the constants in one term requires readjustment in other terms to keep a good description of the single-particle spectrum.

In Ref. [11], the microscopic-macroscopic (MM) and self-consistent methods were related by incorporating the self-consistently derived mean-field potentials [12,13] into the

MM method. These potentials determined under the constraint that we obtain an effective wave equation with a kinetic energy operator containing only a constant mass term in order to comply with the MM method.

The relativistic EDF or relativistic mean-field (RMF) provides us with a functional form of the spin-orbit potential related to the corresponding effective mass. This form was used in Ref. [14] to obtain the spin-orbit mean-field potential in terms of the effective mass derived from the nonrelativistic Giessen EDF [12,13]. Then the mean-field potential was used in the MM approach to study the superheavy nuclei with $Z = 112 - 126$. The impact of the derived spin-orbit potential on the splitting of single-particle levels and nuclear binding energy is the subject of the present paper.

The derivation of the general EDF from the zero-range two-body tensor force was discussed in Refs. [8,9,15,16]. In Ref. [17], a complete fit of the Skyrme EDF with tensor interaction was performed. As pointed out in Ref. [15], some spin-orbit splittings in spherical nuclei can be described better if a tensor force is taken into account. The relative shift of the proton $1g_{7/2}$ and $1h_{11/2}$ levels in tin isotopes is a good test for spin-orbit and tensor interactions. To exclude the effect of pairing correlations, we consider the spin-orbit splitting between the levels that are both above or below the shell gap. In Ref. [18], the relation between the spin-orbit potential and the effective nucleon mass $m^*(r)$ was established. This means that the parameter W_0 in the Skyrme EDF without tensor force is strictly related to the parameters t_1 , t_2 , and x_2 on which the value of m^* at saturation density depends [19–21]. In this paper, we are going to test whether this relation, which should be included in the EDF, provides a good description of spin-orbit splitting and other nuclear properties. Since the spin-orbit splitting depends on both spin-orbit and tensor interactions, we consider the Skyrme EDF with the tensor force. Also, one should check if the rigorous relation between the spin-orbit strength and the effective mass does not spoil the description of the charge radii with various Skyrme EDF. We are going to investigate if there is correlation between the effective mass

and spin-orbit strength in the existing Skyrme EDF without the J^2 terms. Other goal is to demonstrate the role of tensor force in the description of spin-orbit splitting.

The EDF approaches describe quite successfully the binding energies, nuclear shapes, and sizes of nuclei, see, e.g., [18,22–28]. However, they suffer from the uncertainty of the EDF parameters. Indeed, there are various EDF parametrizations, and each of them is most suitable for describing a specific data set. For exploratory studies of the superheavy and exotic nuclei, one should have the EDF with a smaller number of parameters to estimate reliably the shell evolution as a function of the mass (charge) number. The number of parameters can be reduced if there are correlations between them. One can also use the successful MM approach to associate its parameters with the EDF and limit the scope of parameter changes.

The paper is organized as follows. In the next section, a theoretical approach is applied to establish the correlation between effective mass and spin-orbit strength. In Sec. III, the calculated results are presented. Finally, we summarize our work in Sec. IV.

II. RELATIONSHIP BETWEEN SPIN-ORBIT POTENTIAL AND EFFECTIVE MASS

Self-consistent approaches lead to the mean-field potential $V_q + V_{ls}^q$ to be used in the equation for the single-particle wave function ψ_q :

$$\left(-\nabla \cdot \frac{\hbar^2}{2m_q^*(\mathbf{r})} \nabla + V_q(\mathbf{r}) + V_{ls}^q(\mathbf{r}) - \varepsilon_q\right) \psi_q(\mathbf{r}) = 0, \quad (1)$$

where the effective nuclear mass m_q^* ($q = n$ for neutron and $q = p$ for proton) is density dependent and V_{ls}^q the spin-orbit potential written separately from the central potential V_q . Reducing Eq. (1) to the standard Schrödinger equation as in Ref. [11], we obtain

$$\left(-\frac{\hbar^2}{2m_q} \nabla^2 + U_q(r) + U_{ls}^q(r) - \varepsilon_q\right) \psi_q(r) = 0, \quad (2)$$

where the expression for $U_q(r)$ is given in Ref. [11] and

$$U_{ls}^q(r) = \frac{m_q^*(r)}{m_q} V_{ls}^q(r). \quad (3)$$

Due to the density dependence of m_q^* in self-consistent approaches, there is a repulsive correction term to the bare self-consistent mean-field potential V_q . So the equivalent potential $U_q(r)$ is less deep than the self-consistent bare potential and together with $U_{ls}^q(r)$ can be related to the single-particle potential for the Schrödinger equation with bare nucleon mass, which is used in the MM approach. Thus, further conclusions about V_{ls}^q may be related to U_{ls}^q in the MM approach.

In Eq. (1), the spin-orbit potential arises from the corresponding part of the EDF. In the nonrelativistic EDF, this part, which is defined in terms of isoscalar and isovector interactions and corresponding spin currents, requires some parameters. However, in the RMF, the spin-orbit potential consistently appears and it is strictly related to the

difference of the scalar \mathcal{S}_q and vector \mathcal{V}_q parts while the central potential $V_q = \mathcal{S}_q + \mathcal{V}_q$. Thus, in the RMF theory, the central and spin-orbit single-particle self-energies are determined in a unified manner by the same set of scalar and vector fields. The quantity relevant for the spin-orbit potential is the effective mass $m_q^*(r)$, including the Dirac mass and the sum of scalar and vector Dirac self-energies (plus a minor state-dependent constant energy term) [11,29]. In the nonrelativistic limit, $m_q^*(r)$ becomes the nuclear effective mass in Eq. (1).

In the RMF, the projection onto the upper component of the Dirac function results in the Schrödinger equation [18] with the effective mass (in units $\hbar = c = 1$)

$$m_q^*(r) = m_q - \frac{1}{2}[\mathcal{V}_q - \mathcal{S}_q] \quad (4)$$

and the spin-orbit term

$$V_{ls}^q = \frac{1}{(2m_q)^2} (\nabla v_{ls}^q) \cdot (\mathbf{p} \times \sigma), \quad (5)$$

where

$$v_{ls}^q = \frac{m_q}{m_q^*(r)} [\mathcal{V}_q - \mathcal{S}_q] = \frac{2m_q}{m_q^*(r)} [m_q - m_q^*(r)]. \quad (6)$$

In the case of spherical symmetry, the spin-orbit term in Eq. (1) has the following form [30,31]:

$$V_{ls}^q(r) = \frac{1}{2m_q^2} \left(\frac{1}{r} \frac{\partial}{\partial r} v_{ls}^q(r) \right) \mathbf{l} \cdot \mathbf{s} = \left(\frac{1}{r} \frac{\partial}{\partial r} \frac{1}{m_q^*(r)} \right) \mathbf{l} \cdot \mathbf{s}. \quad (7)$$

In the Skyrme mean-field Hamiltonian for nuclear matter with density $\rho(r)$ [32,33],

$$\frac{1}{m_q^*(r)} = \frac{1}{m_q} + \frac{1}{4} ([t_1(2+x_1) + t_2(2+x_2)]\rho(r) - [t_1(1+2x_1) - t_2(1+2x_2)]\rho_q(r)) \quad (8)$$

and

$$V_{ls}^{q\text{Sk}}(r) = \left(\frac{W_0}{2} \frac{\partial}{\partial r} (2\rho_q + \rho_{q'}) + (\alpha J_q + \beta J_{q'}) \right) \frac{1}{r} \mathbf{l} \cdot \mathbf{s} \quad (9)$$

are the effective mass and spin-orbit potential, respectively. Here t_i , x_i , $i = 1, 2$, W_0 are the parameters used in the Skyrme EDF, ρ_q , and J_q are the nucleon and spin-orbit densities, respectively. If $q = n$, then $q' = p$ and vice versa. So $\rho = \rho_q + \rho_{q'}$ is the total nucleon density. The values of α and β can be separated into contributions from the central force (α_c, β_c) and the tensor force (α_T, β_T) [8,34]. The central part (α_c, β_c) effectively renormalizes the value of W_0 for spin-unsaturated nuclei [15,35], where

$$\alpha_c = \frac{1}{8}(t_1 - t_2) - \frac{1}{8}(t_1x_1 + t_2x_2), \quad \beta_c = -\frac{1}{8}(t_1x_1 + t_2x_2). \quad (10)$$

However, the tensor force appreciably contributes to the spin-orbit splitting of single-particle levels and the J^2 terms should be considered in addition to the effect of the value of W_0 . Here we have two main objectives. The first is to relate Eqs. (7) and (9) in the absence of a tensor force, which is not present in Eq. (7). The second goal is to demonstrate the significant

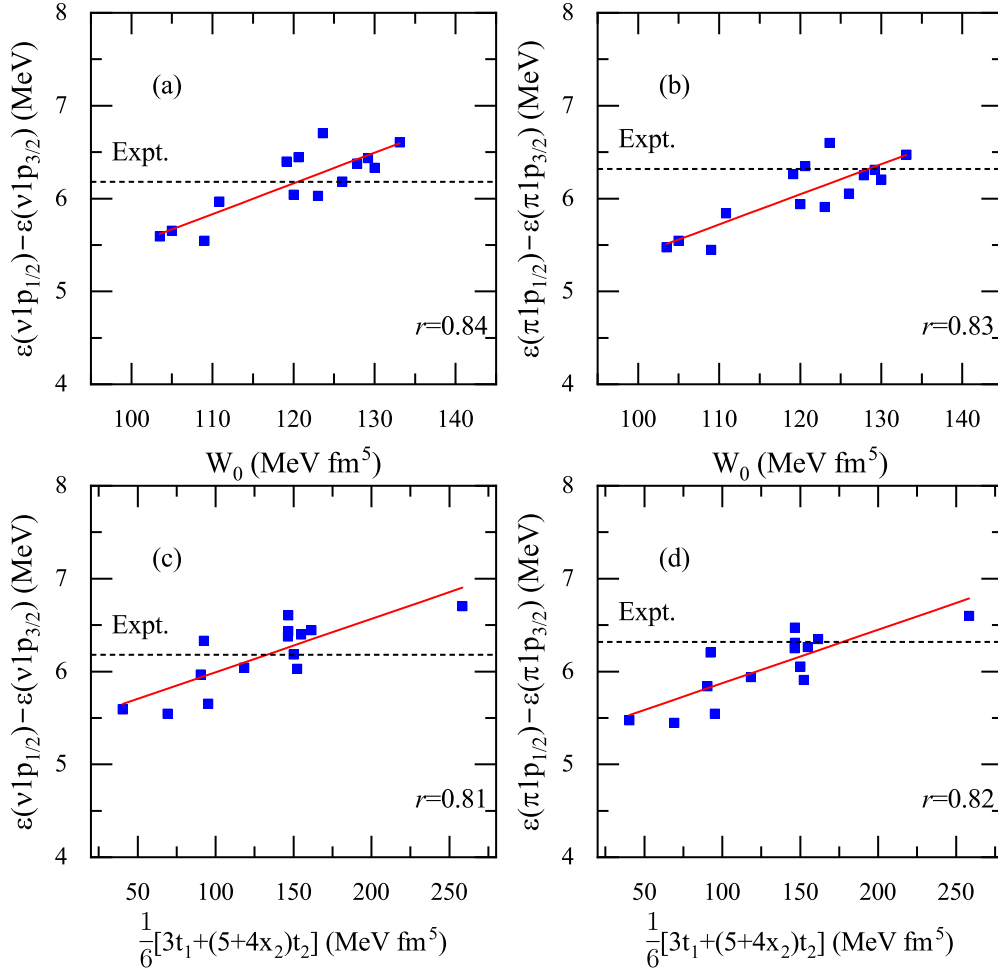


FIG. 1. Spin-orbit splitting for the neutron [(a) and (c)] and proton [(b) and (d)] $1p$ states in ^{16}O versus the value of spin-orbit potential W_0 [(a) and (b)] or versus the value of $\frac{1}{6}[3t_1 + (5 + 4x_2)t_2]$ [(c) and (d)] calculated using the 14 Skyrme EDFs. The correlation coefficients are shown. The experimental values of the spin-orbit splitting for $1p$ states are 6.18 and 6.32 MeV for neutron and proton [42], respectively.

role of tensor force in the Skyrme EDF for describing isotopic dependence of spin-orbit splitting.

Notice that the in-medium effective mass m^* can be recognize by considering the two contributions to m^* : the k mass, which is also called the nonlocality mass, and the ω mass, which is induced by dynamical correlations such as particle-vibration coupling (PVC) [36–41]. As shown in Refs. [39–41], the PVC, which is beyond mean-field correlations, affects the strength of the spin-orbit splitting in the same way as the tensor force, which is a part of the nucleon-nucleon interaction, i.e., two effects of different origin improve the description of experimental data [40]. While in the RMF [39,41] only the PVC is introduced, in the Skyrme EDF it is considered in addition to the tensor force [40]. So if we would like to compare the spin-orbit potentials in the RMF and Skyrme EDF, we should compare Eqs. (7) and (9) without the J^2 terms.

In the Skyrme EDF, the effective mass is model dependent. However, it should be of the same origin as in the RMF model. Therefore, the first part of Eq. (9) can be compared with Eq. (7) taking Eq. (8) into account. Equating the Skyrme and RMF effective masses and the spin-orbit potentials

depending only on the densities ρ_q , we obtain

$$\begin{aligned} \frac{1}{2}W_0[\rho(r) + \rho_q(r)] &= \frac{1}{4}([t_1(2 + x_1) + t_2(2 + x_2)]\rho(r) \\ &\quad - [t_1(1 + 2x_1) - t_2(1 + 2x_2)]\rho_q(r)). \end{aligned} \quad (11)$$

Summing these expressions for protons and neutrons, we obtain the relationship

$$W_0 = \frac{1}{6}[3t_1 + (5 + 4x_2)t_2] \quad (12)$$

between the constants of the Skyrme EDF and express the Skyrme spin-orbit potential in the form of Eq. (7).

To study the role of the spin-orbit potential in the EDF, it is interesting to look at single-particle spectra, in particular because they provide us information on the strength of the spin-orbit splitting. Let us consider the neutron and proton $1p_{1/2} - 1p_{3/2}$ splitting in ^{16}O as the most popular example of the studies of the spin-orbit potential in atomic nucleus [8,21,32]. Figure 1 shows that the calculated spin-orbit splitting for the 14 Skyrme EDFs without tensor part are in reasonable agreement with experimental data [42]. As seen, for neutron and proton $1p_{1/2} - 1p_{3/2}$ splitting there is a

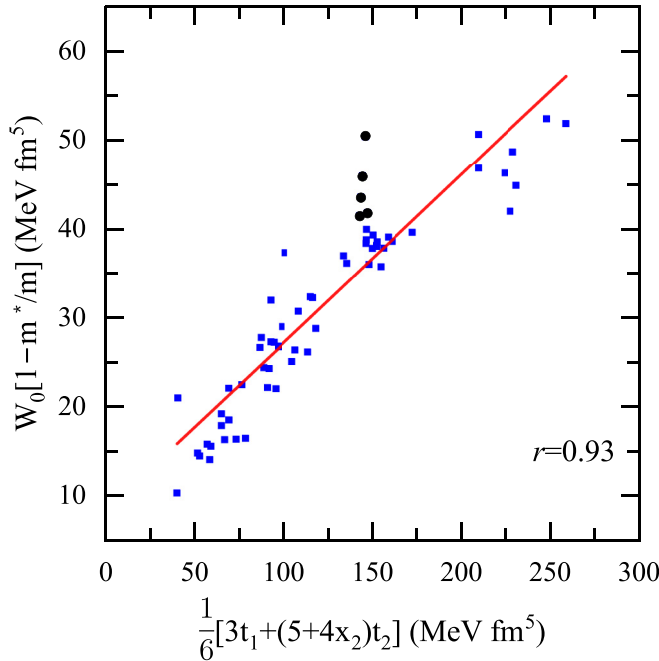


FIG. 2. The product of the spin-orbit coupling constant W_0 and the value of $(1 - m^*/m)$ versus the value of $\frac{1}{6}[3t_1 + (5 + 4x_2)t_2]$ calculated using various Skyrme EDF (filled squares). A correlation coefficient $r = 0.93$ is found. Filled circles correspond to the EDFs with tensor part.

correlation with the value of W_0 . However, we can consider the dependence of splitting on the right-hand side of Eq. (12). Our results exhibit a direct relationship between spin-orbital splitting and the values of $\frac{1}{6}[3t_1 + (5 + 4x_2)t_2]$. Thus, using the example of ^{16}O , we demonstrate the obvious correlation between the values of W_0 and $\frac{1}{6}[3t_1 + (5 + 4x_2)t_2]$. As a result, we would expect a strong correlation between the value of W_0 and the parameters t_1 , t_2 , and x_2 on which the effective mass at saturation density depends. It should be noted that according to the effective field theories there is a direct relationship between the spin-orbital splitting and the effective nucleon mass; see, e.g., Refs. [32,43].

To check if there is a correlation between the values of W_0 and $\frac{1}{6}[3t_1 + (5 + 4x_2)t_2]$ in the existing Skyrme EDF, we show in Fig. 2 $\frac{1}{6}[3t_1 + (5 + 4x_2)t_2]$ versus $W_0(1 - m^*/m)$ for various Skyrme EDF (see Ref. [44] for original references). Here m^* is an effective mass at saturation density. There is a set of EDF with the effective mass close to the bare mass m , which leads to almost zero $\frac{1}{6}[3t_1 + (5 + 4x_2)t_2]$. If m^* deviates from m by more than 10%, the values of $\frac{1}{6}[3t_1 + (5 + 4x_2)t_2]$ are close to the adjusted values of the spin-orbit coupling constant W_0 . In Fig. 2, there is deviation of points from the line because Eq. (12) was not used in the multiparameter fitting procedure and W_0 was independent parameter. However, in Fig. 2 most of the points are in a narrow strip around the line. In Fig. 2, we marked points corresponding to the EDFs of the TIJ family with tensor interaction. As expected, these points have a larger deviation from the line because the tensor part is not taken into account in Eq. (12). About 90% of

the considered EDFs (more than 60 parametrizations) without tensor part correspond to points, which are rather close to the line. So the fit of the parameters of the EDF confirms Eq. (12) and the spin-orbit potential can be found with Eq. (7) using the dependence of $m_q^*(r)$ on r .

III. RESULTS AND DISCUSSIONS

A. Details of calculations

The starting point of the method is the Hartree-Fock (HF)-BCS calculation [45] of the ground state based on Skyrme EDFs. Spherical symmetry is imposed on the quasiparticle wave functions for the nuclei considered here. The continuous part of the single-particle spectrum is discretized by diagonalizing the Skyrme HF Hamiltonian in a harmonic oscillator basis. This method could be extended to the HFB framework in the canonical quasiparticle basis. In the particle-hole channel, we use the Skyrme EDFs with the tensor terms, which modify the spin-orbit potential [8,15] [see Eq. (9)].

Except for double-magic nuclei, we perform HF-BCS calculations in order to take into account pairing correlations. Pairing correlations are generated by the density-dependent zero-range force

$$V_{\text{pair}}(\mathbf{r}_1, \mathbf{r}_2) = V_0 \left(1 - \eta \left(\frac{\rho(r_1)}{\rho_0} \right)^\gamma \right) \delta(\mathbf{r}_1 - \mathbf{r}_2), \quad (13)$$

where $\rho(r_1)$ is the particle density in coordinate space, and ρ_0 is the nuclear matter saturation density. The parameters $V_0 = 870 \text{ MeV fm}^3$, $\eta = 1$, and $\gamma = 1$ are fixed in Ref. [46] along the Sn isotopic chain for the SLy4 EDF. It was checked that the same parameters can be used with the SLy5 EDF. The parameters of the SLy5 EDF were adjusted to reproduce nuclear matter properties as well as nuclear charge radii and binding energies of doubly magic nuclei [21]. Also, in the particle-hole channel, we use the Skyrme EDF SLy5+T in which the tensor term is added without refitting the parameters of the central interaction [34]. In the family of TIJ parametrizations [8], covering a wide range of parameters of the isoscalar and isovector tensor terms, the parameters of the central interaction are refitted using a fit protocol similar to that of the successful SLy parametrizations. It should be noted that the HF-BCS results for the TIJ parametrizations are obtained with the same value of the pairing strength V_0 as for the SLy5 or SLy5+T EDFs.

B. Isotopic dependence of energy difference between single-particle levels

First, we examine the role of the spin-orbit coupling constant W_0 in the single-particle spectrum using the available experimental data [47] for the single-particle states in $Z = 50$ isotopes and $N = 82$ isotones.

Energy space between the proton $1h_{11/2}$ and $1g_{7/2}$ levels for the chain of tin isotopes is presented in Fig. 3. The experimental data are compared with the calculated results obtained with the SLy5 EDF without and with tensor force introduced with the parameters $(\alpha_T, \beta_T) = (-170, 100) \text{ MeV fm}^5$. As seen in Fig. 3, the inclusion of the condition (12) in the HF-BCS calculations with the original SLy5 EDF (SLy5m

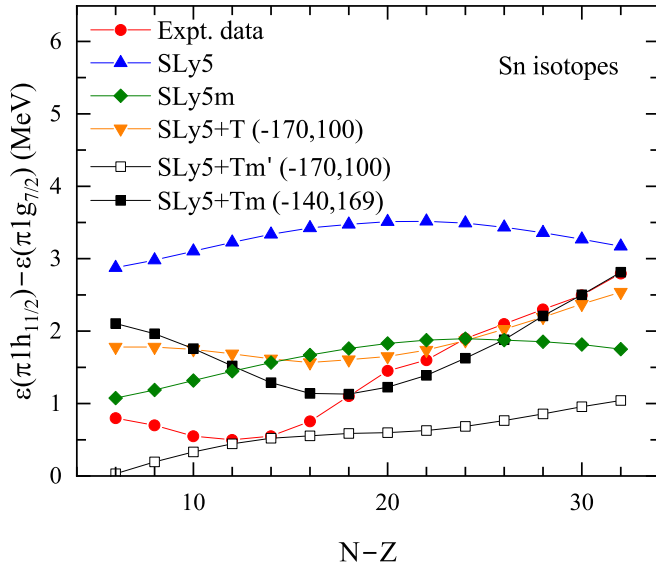


FIG. 3. Energy differences between the proton $1h_{11/2}$ and $1g_{7/2}$ levels along the tin isotopes. The experimental data are taken from Ref. [47]. See the text for details.

EDF in Fig. 3) predicts only an overall decrease in the energy differences between the proton $1h_{11/2}$ and $1g_{7/2}$ levels (from 1.4 MeV for ^{132}Sn to 1.8 MeV for ^{106}Sn), while maintaining the behavior of the curve calculated with the SLy5 EDF. Due to the modification of the parameter W_0 in the SLy5m EDF, we only change the parameter $t_0 = -2482.0 \text{ MeV fm}^3$ to keep the nuclear binding energy. Thus, increasing the value of W_0 through the relationship (12) is not enough for a correct description of the isotopic dependence of experimental data, and tensor correlations need to be taken into account. In the case of the SLy5+T EDF, the inclusion of the tensor force in the EDF improves the description of level splitting, but

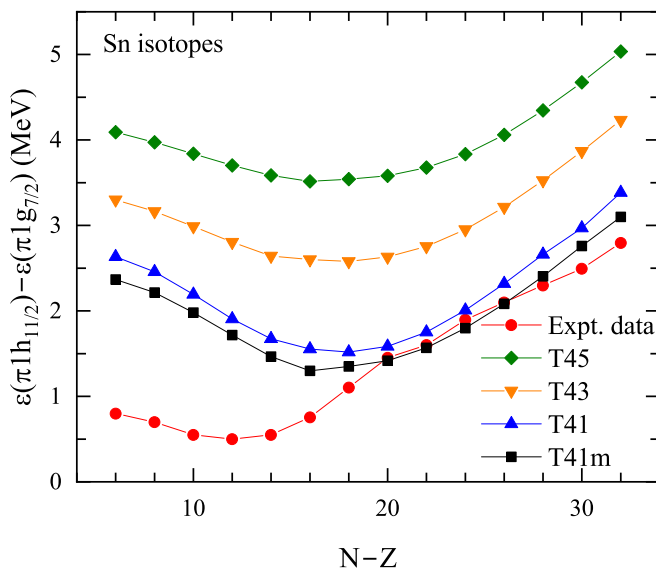


FIG. 4. The same as in Fig. 3 but for the T41, T41m, T43, and T45 EDFs.

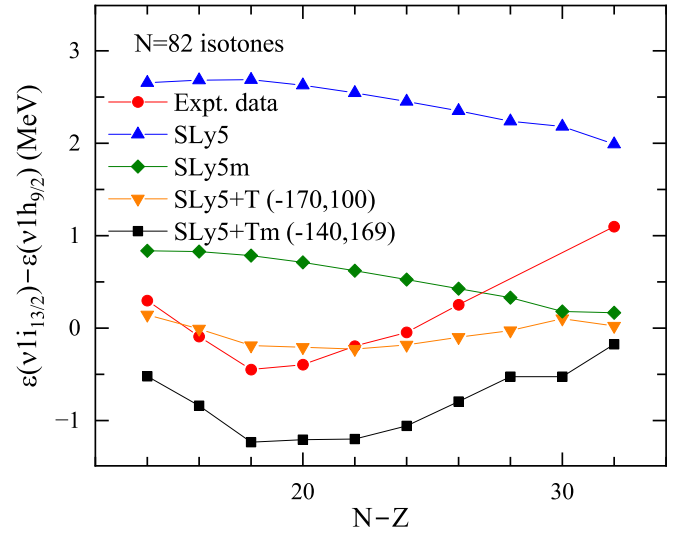


FIG. 5. Energy differences between the neutron $1i_{13/2}$ and $1h_{9/2}$ levels along the $N = 82$ isotones. The experimental data are taken from Ref. [47]. See the text for details.

the deflection of the calculated curve in the case of light tin isotopes is still smaller than the experimental one. As seen, if we impose the condition (12), the value of W_0 increases from 126.0 to 149.9 MeV fm^5 . As a result of growing the spin-orbit potential by almost 20%, the energy differences between the proton $1h_{11/2}$ and $1g_{7/2}$ levels is shifted down by 1.1–1.8 MeV (see curve SLy5+Tm' in the Fig. 3) and significantly worsens the description of the data. To restore the quality of description obtained with the SLy5+T EDF, we refit the values of $(\alpha_T, \beta_T) = (-140, 169) \text{ MeV fm}^5$. As seen in Fig. 3, the HF-BCS calculations within the SLy5+Tm EDF well reproduce the SLy5+T results. It is worth mentioning that we change the Skyrme parameter $t_0 = -2482.5 \text{ MeV fm}^3$ to maintain the description of nuclear binding energy without readjustment of other parameters of the original set of SLy5

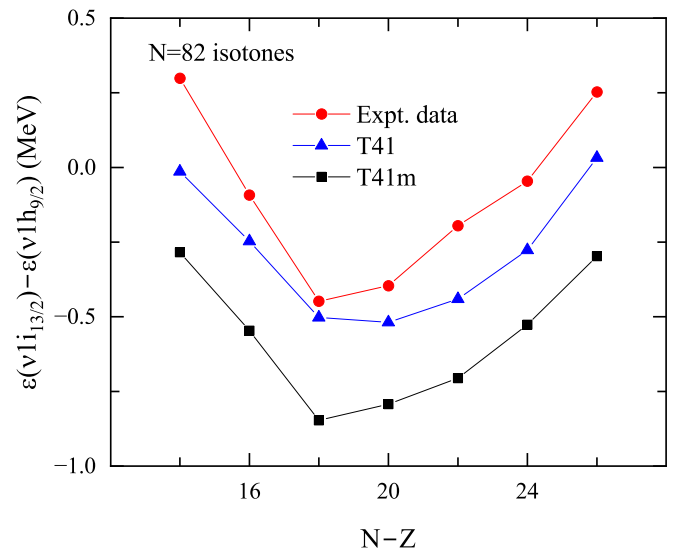


FIG. 6. The same as in Fig. 5 but for the T41 and T41m EDF's.

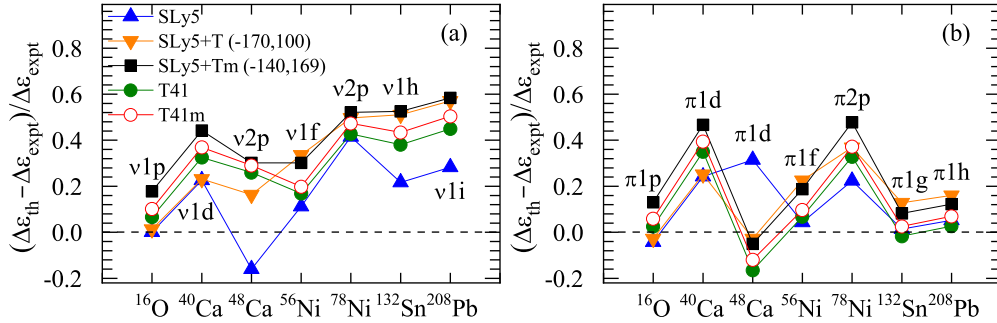


FIG. 7. Relative error of the spin-orbit splittings for the (a) neutron and (b) proton levels in doubly magic nuclei. The experimental data are taken from Ref. [42]. See the text for details.

with the condition (12). The necessity of this adjustment following the change of W_0 confirms the correlation of the parameters in the spin-orbit and tensor parts of the EDF.

Depending on the nature of the tensor terms in the EDF (i.e., like-particle or proton-neutron or a mixture of both) [8], the spin-orbit current contributes to the spin-orbit potential of neutrons or to that of protons or to both [see Eq. (9)]. The family of TIJ parametrizations allows us to describe these contributions. Let us consider as an example the following T41, T43, and T45 EDFs in which different values of the coupling constants in the tensor terms lead to a qualitative description of the isotopic dependence of energy differences between the proton $1h_{11/2}$ and $1g_{7/2}$ levels. As shown in Fig. 4, with a decrease in the strength of the coupling constants of the like-particle tensor terms, the calculated results approach the experimental values. Among the T41, T43, and T45 EDFs with the tensor force, the T41 EDF describes better the splitting of the proton $1h_{11/2}$ and $1g_{7/2}$ levels. In the case of the T41m EDF, in which W_0 in the T41 EDF is from Eq. (12) and the Skyrme parameter t_0 is changed from $-2492.261 \text{ MeV fm}^3$ to -2491.7 MeV fm^3 , the description of the experimental data becomes even better. So the relationship (12) allows us to reduce the number of parameters in the EDF without losing the quality of description.

Let us now discuss the impact the spin-orbit coupling constant W_0 on the single-particle spectrum in the case of $N = 82$

isotones. Energy space between the neutron $1i_{13/2}$ and $1h_{9/2}$ levels for the chain of $N = 82$ isotones as a function of the neutron excess is presented in Fig. 5. As seen, the tensor force in SLy5 EDF improves the calculated results. The use of Eq. (12) in addition leads to the curves almost equidistant to the experimental one. The shift between these curves can probably be reduced by adjusting other EDF parameters that is outside of the main goal of the work to investigate if there is correlation between the effective mass and spin-orbit strength in the existing Skyrme EDF. One can see that the HF-BCS calculations with the SLy5m EDF, in which the spin-orbit constant W_0 in the SLy5 EDF is modified by using Eq. (12), lead only to a shift of the curve down about 1.8–1.9 MeV. As a result, the calculated curve does not describe well the experimental data. In the case of the T41m EDF, in which the value of W_0 is taken from Eq. (12), we do not change the trend of the level splitting depending on $N - Z$, just slightly shifting the curve down (see Fig. 6).

The energy space between the levels that are both above or both below the magic gap are not much affected by polarization and correlation effects [8]. Figure 7 displays the relative errors of the calculated single-particle splitting of such states in doubly magic spherical nuclei ^{16}O , $^{40,48}\text{Ca}$, $^{56,78}\text{Ni}$, ^{132}Sn , and ^{208}Pb . The calculated values are typically 20–40% larger than the experimental ones, with the exception of ^{16}O , where the splittings of the neutron and proton $1p$ states are well

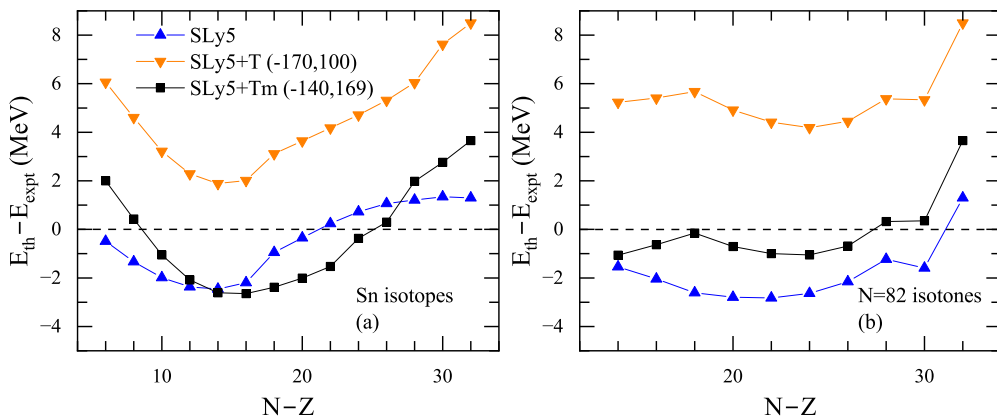


FIG. 8. Binding energy difference $E_{\text{th}} - E_{\text{expt}}$ along (a) $Z = 50$ isotopic and (b) $N = 82$ isotonic chains for the parametrizations indicated. Positive values of $E_{\text{th}} - E_{\text{expt}}$ denote overbound nuclei and negative values denote underbound nuclei. The experimental data are taken from Ref. [48].

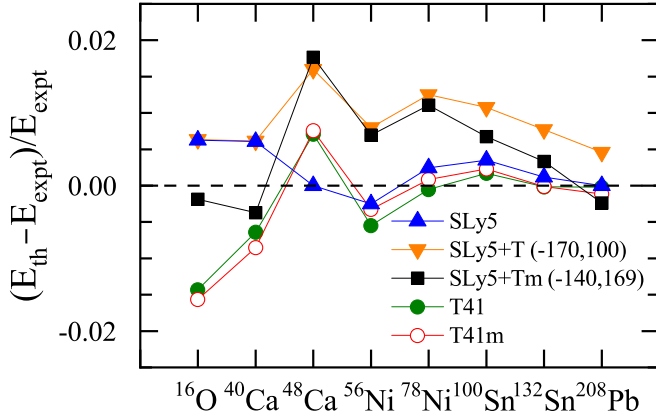


FIG. 9. Relative errors in binding-energy estimates of doubly magic nuclei. The experimental data are taken from Ref. [48].

reproduced. As seen, the use of Eq. (12) with some adjustment in the tensor part of the EDF increases the relative errors within 10% but maintains the general trend. Thus, Eq. (12) provides reasonable values of spin-orbit strengths.

C. Binding energy and charge radius

Let us now consider the binding energy. Figure 8 displays the differences $E_{\text{th}} - E_{\text{expt}}$ between the calculated and experimental binding energies along the $Z = 50$ isotopic and $N = 82$ isotonic chains. Positive values of $E_{\text{th}} - E_{\text{expt}}$ denote overbound nuclei and negative values denote underbound nuclei. The inclusion of the tensor term into the SLy5 EDF leads to an overestimation of the binding energy by a few MeV but qualitatively preserves the dependence of the binding energy on the neutron excess $N - Z$. Due to the modification of the spin-orbit coupling constant W_0 in the case of the SLy5+T EDF, we change the parameter t_0 to keep the binding energy. As a result, the SLy5+Tm EDF give a reasonable description of the experimental energies. So taking into account Eq. (12), one can perhaps get a similar quality of description of the binding energy and single-particle splittings as in the case of the EDF with W_0 as an independent parameter.

The relative errors in binding-energy estimates for magic nuclei are shown in Fig. 9 for the considered EDFs with and without the tensor force and condition (12). As seen, the condition (12) does not spoil the quality of description of the binding energy, which is within 2%.

Let us examine the rms charge radii $\langle R_{\text{ch}}^2 \rangle^{1/2}$. The nuclear charge radii are related to the rms point-proton radii with their correction for the finite charge distributions of protons and neutrons, as well as for the Darwin-Foldy term, and the spin-orbital correction (see, for example, Ref. [49]). In this study, the charge radius of a nucleus can be approximated by the following empirical expression:

$$\langle R_{\text{ch}}^2 \rangle \approx \langle R_p^2 \rangle + 0.64 \text{ fm}^2, \quad (14)$$

where $\langle R_p^2 \rangle^{1/2}$ is the rms proton radius. This estimate gives an error of about 0.02 fm compared to more accurate calculations of the charge radius [49].

The evolution of nuclear charge radii along the Sn isotopic chain reflects how the mean field of the protons changes when neutrons are added to the system. In the MM models [50], this effect is reflected in the geometrical growth of the size of nucleus and in the isotopic dependence of the parameters of the microscopic and liquid-drop parts. As seen in Fig. 10(a), the quality of description is almost the same in the cases of the EDF with and without the tensor interaction. Imposing the condition (12), we obtain as good description of charge radii as in the case of the independent parameter W_0 . The same conclusion can be found from the analysis of the calculated results in the case of $N = 82$ isotones; see Fig. 10(b).

In Table I, we compare the charge radii $\langle R_{\text{ch}}^2 \rangle^{1/2}$ of doubly magic nuclei from different measurements. They are in good agreement, within 0.01 fm. For ^{56}Ni , there is only one measurement [53]. We also show in Table I the charge radii predicted within the considered EDFs and explore the impact of changing spin-orbit strength in accordance with condition (12). As for the absolute radii, in Table I there is a minor variation between the values obtained with different EDF.

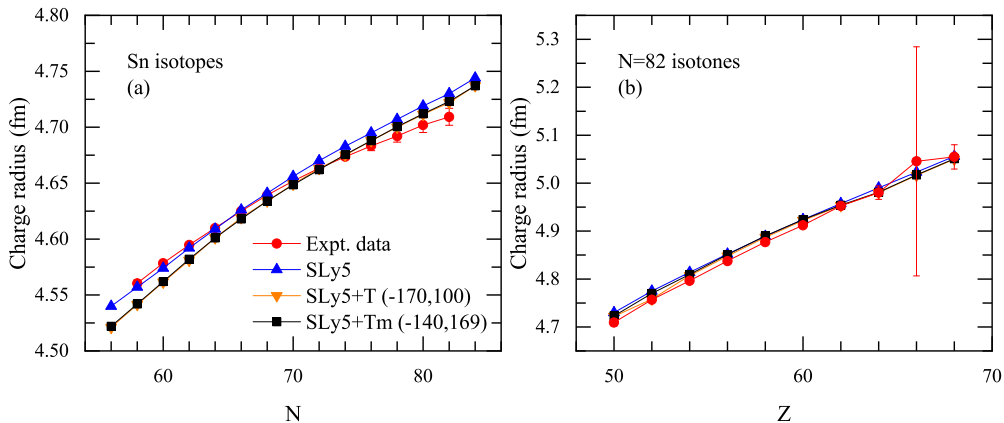


FIG. 10. The rms charge radii along the (a) $Z = 50$ isotopic and (b) $N = 82$ isotonic chains for the parametrizations indicated. The experimental data are taken from Ref. [51]. The total error bars are almost within the size of symbols expecting the case of $Z = 66, 68$ and $N = 82$.

TABLE I. Comparison of experimental charge radii based on the results of various measurements [51–53] with those calculated with the indicated EDFs.

Nucleus	Expt. data			Theory				
	Ref. [52]	Ref. [51]	Ref. [53]	SLy5	SLy5+T	SLy5+Tm	T41	T41m
¹⁶ O	2.730(25)	2.6991(52)	–	2.800	2.800	2.806	2.815	2.816
⁴⁰ Ca	3.478(1)	3.4776(19)	–	3.508	3.508	3.515	3.516	3.518
⁴⁸ Ca	3.474(1)	3.4771(20)	–	3.542	3.532	3.529	3.534	3.533
⁵⁶ Ni	–	–	3.7226(27)	3.783	3.772	3.770	3.780	3.781
¹³² Sn	–	4.7093(76)	–	4.730	4.722	4.723	4.725	4.724
²⁰⁸ Pb	5.501(1)	5.5012(13)	–	5.508	5.502	5.505	5.499	5.499

IV. SUMMARY

Extraction of the spin-orbit potential from the EDF without tensor force resulted in the relationship between the spin-orbit strength and the nucleon effective mass at saturation density. The correlation between the values of W_0 and m^* was demonstrated in various Skyrme EDF. This correlation can help us to reduce the number of parameters used in the EDF and relate the nonrelativistic and relativistic EDFs.

The role of the spin-orbit interaction was considered together with the tensor force since these interactions affect the same observed quantities. As shown, the tensor force consid-

erably improves the description of the isotopic dependence of the spin-orbit splitting. The use of the relation between W_0 and m^* in the Skyrme EDF does not spoil the description of experimental data. It even leads to a better description of the nuclear binding energies.

ACKNOWLEDGMENTS

The research was supported in the framework of the scientific program of the National Center for Physics and Mathematics, topic No. 6 “Nuclear and radiation physics” (2023–2025 stage).

-
- [1] M. Goeppert Mayer, *Phys. Rev.* **74**, 235 (1948).
[2] O. Haxel, J. H. D. Jensen, and H. E. Suess, *Phys. Rev.* **75**, 1766 (1949).
[3] E. Feenberg and K. C. Hammack, *Phys. Rev.* **75**, 1877 (1949).
[4] A. N. Bezbakh, G. G. Adamian, and N. V. Antonenko, *Phys. Rev. C* **105**, 054305 (2022).
[5] M. Beiner, H. Flocard, N. V. Giai, and P. Quentin, *Nucl. Phys. A* **238**, 29 (1975).
[6] J. Dobaczewski, I. Hamamoto, W. Nazarewicz, and J. A. Sheikh, *Phys. Rev. Lett.* **72**, 981 (1994).
[7] G. A. Lalazissis, D. Vretenar, W. Pöschl, and P. Ring, *Phys. Lett. B* **418**, 7 (1998).
[8] T. Lesinski, M. Bender, K. Bennaceur, T. Duguet, and J. Meyer, *Phys. Rev. C* **76**, 014312 (2007).
[9] H. A. Bethe, *Phys. Rev.* **167**, 879 (1968).
[10] J. W. Negele, *Phys. Rev. C* **1**, 1260 (1970).
[11] G. G. Adamian, L. A. Malov, N. V. Antonenko, H. Lenske, K. Wang, and S.-G. Zhou, *Eur. Phys. J. A* **54**, 170 (2018).
[12] H. Lenske and C. Fuchs, *Phys. Lett. B* **345**, 355 (1995).
[13] F. Hofmann and H. Lenske, *Phys. Rev. C* **57**, 2281 (1998).
[14] L. A. Malov, G. G. Adamian, N. V. Antonenko, and H. Lenske, *Phys. Rev. C* **104**, 064303 (2021).
[15] F. Stancu, D. M. Brink, and H. Flocard, *Phys. Lett. B* **68**, 108 (1977).
[16] F. Tondeur, *Phys. Lett. B* **123**, 139 (1983).
[17] K.-F. Liu, H. Luo, Z. Ma, Q. Shen, and S. A. Moszkowski, *Nucl. Phys. A* **534**, 1 (1991).
[18] P. Ring, *Prog. Part. Nucl. Phys.* **37**, 193 (1996).
[19] D. Vautherin and D. M. Brink, *Phys. Rev. C* **5**, 626 (1972).
[20] N. V. Giai and H. Sagawa, *Phys. Lett. B* **106**, 379 (1981).
[21] E. Chabanat, P. Bonche, P. Haensel, J. Meyer, and R. Schaeffer, *Nucl. Phys. A* **635**, 231 (1998); **643**, 441(E) (1998).
[22] G. A. Lalazissis, D. Vretenar, and P. Ring, *Phys. Rev. C* **57**, 2294 (1998).
[23] S. A. Fayans, S. V. Tolokonnikov, E. L. Trykov, and D. Zawischa, *Nucl. Phys. A* **676**, 49 (2000).
[24] M. Bender, P.-H. Heenen, and P.-G. Reinhard, *Rev. Mod. Phys.* **75**, 121 (2003).
[25] S.-G. Zhou, J. Meng, and P. Ring, *Phys. Rev. C* **68**, 034323 (2003).
[26] D. Vretenar, A. V. Afanasjev, G. A. Lalazissis, and P. Ring, *Phys. Rep.* **409**, 101 (2005).
[27] M. Baldo, P. Schuck, and X. Viñas, *Phys. Lett. B* **663**, 390 (2008).
[28] J. Meng and S.-G. Zhou, *J. Phys. G: Nucl. Part. Phys.* **42**, 093101 (2015).
[29] G. G. Adamian, N. V. Antonenko, H. Lenske, L. A. Malov, and S.-G. Zhou, *Eur. Phys. J. A* **57**, 89 (2021).
[30] N. Van Giai and L. N. Savushkin, *Sov. J. Part. Nucl.* **23**, 373 (1992).
[31] M. López-Quelle, N. Van Giai, S. Marcos, and L. N. Savushkin, *Phys. Rev. C* **61**, 064321 (2000).
[32] P.-G. Reinhard, *Rep. Prog. Phys.* **52**, 439 (1989).
[33] G. Colò, N. V. Giai, and H. Sagawa, *Phys. Lett. B* **363**, 5 (1995).
[34] G. Colò, H. Sagawa, S. Fracasso, and P. F. Bortignon, *Phys. Lett. B* **646**, 227 (2007); **668**, 457(E) (2008).
[35] S. Fracasso and G. Colò, *Phys. Rev. C* **76**, 044307 (2007).
[36] N. Vinh Mau and A. Bouyssy, *Nucl. Phys. A* **257**, 189 (1976).
[37] V. Bernard and N. V. Giai, *Nucl. Phys. A* **348**, 75 (1980).
[38] Z. Y. Ma and J. Wambach, *Nucl. Phys. A* **402**, 275 (1983).
[39] E. Litvinova and P. Ring, *Phys. Rev. C* **73**, 044328 (2006).
[40] G. Colò, H. Sagawa, and P. F. Bortignon, *Phys. Rev. C* **82**, 064307 (2010).

- [41] E. V. Litvinova and A. V. Afanasjev, *Phys. Rev. C* **84**, 014305 (2011).
- [42] H. Grawe, K. Langanke, and G. Martínez-Pinedo, *Rep. Prog. Phys.* **70**, 1525 (2007).
- [43] R. J. Furnstahl, J. J. Rusnak, and B. D. Serot, *Nucl. Phys. A* **632**, 607 (1998).
- [44] M. Dutra, O. Lourenço, J. S. Sá Martins, A. Delfino, J. R. Stone, and P. D. Stevenson, *Phys. Rev. C* **85**, 035201 (2012).
- [45] P. Ring and P. Schuck, *The Nuclear Many Body Problem* (Springer, Berlin, 1980).
- [46] N. N. Arsenyev and A. P. Severyukhin, *Universe* **7**, 145 (2021).
- [47] J. P. Schiffer, S. J. Freeman, J. A. Caggiano, C. Deibel, A. Heinz, C.-L. Jiang, R. Lewis, A. Parikh, P. D. Parker, K. E. Rehm, S. Sinha, and J. S. Thomas, *Phys. Rev. Lett.* **92**, 162501 (2004).
- [48] M. Wang, W. J. Huang, F. G. Kondev, G. Audi, and S. Naimi, *Chin. Phys. C* **45**, 030003 (2021).
- [49] B. V. Carlson, M. Dutra, O. Lourenço, and J. Margueron, *Phys. Rev. C* **107**, 035805 (2023).
- [50] A. N. Kuzmina, G. G. Adamian, N. V. Antonenko, and W. Scheid, *Phys. Rev. C* **85**, 014319 (2012).
- [51] I. Angeli and K. P. Marinova, *At. Data Nucl. Data Tables* **99**, 69 (2013).
- [52] G. Fricke and K. Heilig, in *Nuclear Charge Radii*, edited by H. Schopper (Springer-Verlag, Berlin, 2004).
- [53] F. Sommer, K. König, D. M. Rossi, N. Everett, D. Garand, R. P. de Groote, J. D. Holt, P. Imgram, A. Incorvati, C. Kalman, A. Klose, J. Lantis, Y. Liu, A. J. Miller, K. Minamisono, T. Miyagi, W. Nazarewicz, W. Nörtershäuser, S. V. Pineda, R. Powel, P.-G. Reinhard, L. Renth, E. Romero-Romero, R. Roth, A. Schwenk, C. Sumithrarachchi, and A. Teigelhöfer, *Phys. Rev. Lett.* **129**, 132501 (2022).